Improving super resolution in time reversal focusing among a resonator array by restricting the angle of incidence

Andrew Basham

A senior thesis submitted to the faculty of

Brigham Young University

in partial fulfillment of the requirements for the degree of

Bachelor of Science

Brian E. Anderson, Advisor

Department of Physics and Astronomy

Brigham Young University

June 2023

ABSTRACT

Improving super resolution in time reversal focusing among a resonator array by restricting the angle of incidence

Andrew Basham

Department of Physics and Astronomy, BYU

Bachelor of Science

Super resolution is possible using resonators placed in the near field of time reversal focusing. A two-dimensional Helmholtz resonator array in a three-dimensional reverberant environment has limited ability to produce a high-resolution spatial focus in the time reversal focusing of audible sound. Acoustic waves propagating out-of-plane with the resonator array are not as strongly affected by the smaller effective wavelength induced by the resonator array, partially negating the effect of the resonators. A physical two-dimensional waveguide is shown to limit the out-of-plane propagation, leading to improved resolution. It is also shown that post processing using an orthogonal particle velocity decomposition of a spatial scan of the focusing can limit out-of-plane particle motion in the near field of the array, which bypasses the effect of the unwanted third spatial dimension of propagation. Each of these techniques results in a pressure field focus reconstruction that has a progressively higher spatial resolution.

Keywords: time reversal, super resolution, metamaterial, resonator array

ACKNOWLEDGMENTS

Funding was provided by the BYU College of Physical and Mathematical Sciences and Los Alamos National Laboratory, subcontract number 527136. Facilities at BYU were used for this research.

I also wish to thank Brian Anderson and the Time Reversal research group for the time and support they put into making my work possible; special thanks to Adam Kingsley for his close collaboration and development of the extremely convenient software ESTR. Finally, thank you to my family for their continual support and for cheering me on from start to finish.

.

Table of Contents

.

List of Figures

Chapter 1

Introduction

Acoustic imaging is the use of acoustic waves to characterize a sound source, such as the ultrasound methods commonly used in medical imaging applications.[1-2] There's an interest in many applications to achieve the highest resolution possible. Acoustic imaging is limited, however, in its ability to resolve point sources from each other in the far field due to the diffraction limit. The diffraction limit has been defined in various ways, but all aiming to define the physical limit of resolution achievable by a propagating wave.[3] Here we use the common definition of the wavelength divided by two, $\lambda/2$, of the full width at half-maximum (FWHM) of the spatial extent of the focusing (or $\lambda/4$ for intensities).[3] For a focus comprised of a finite bandwidth, the strictest definition is to assume λ is the wavelength of the highest frequency of the bandwidth, which we adopt here.

Focusing and imaging are directly related to one another, which makes improvements in focusing techniques an important part of improving imaging applications as well.[1] The method of acoustic focusing used here is time reversal (TR). TR is a signal processing technique that has been employed to focus waves in the electromagnetic, ultrasonic, and aeroacoustic domains.[4-6] Reciprocal TR is performed in a two-step process between emitting transducers and a receiver placed at the desired focal location.[5] The forward step is simply obtaining an impulse response between each emitting transducer and the receiver; the backwards step has each emitting transducer simultaneously play back a time-reversed version of its corresponding impulse response

obtained in the forward step. These emissions time align reflections and direct sound propagation such that they constructively interfere at the receiver position to approximately reconstruct the original impulse. Here a chirp signal is emitted during the forward step and the impulse response is obtained through cross-correlation of the chirp signal and the response to the chirp signal.[7-8]

The first use of TR was for underwater communication applications.[9] TR has subsequently been used in a variety of applications, including underwater,[10-13] airborne,[14-16] and elastic[17] communications, high amplitude focusing[18] for medical applications,[19-21] nondestructive evaluation,[6,22] and of loud sound,[23-26] and source reconstruction and imaging. Source imaging with TR includes application to earthquakes,[27-30] touchpad taps,[31-32] and gunshot localization.[33-34]

Contrary to what is typical with other focusing methods like beamforming, TR excels in reverberant environments and with complex geometries. Not only does it not suffer from such complexity, it actually beneficially exploits a high degree of reverberation to deliver even more coherent energy to the focus by turning reflected sound into virtual sources, thus creating a wider angular aperture. However, even under ideal circumstances the best focus resolution possible for a TR focus is defined by the diffraction limit, $\lambda/2$.[35]

Recent explorations have achieved subwavelength focusing, or super resolution, by the use of an array of resonators in the near field of the focus (though other techniques besides using resonators have been used as well, see reviews in Refs. 36-37). Lerosey *et al.*[38]set up an arrangement of resonating wire antennae and demonstrated $\lambda/30$ resolution (the antenna spacing). Lemoult *et al.*[39-40] then extended this idea to focusing sound among an array of Helmholtz resonators comprised of common soda cans. The emitting transducers were placed equidistant to the intended location of the focus over one of the soda cans (the transducers were in the same plane as the can array) and emitted sound in short pulses, time-aligned using TR. It was shown that this

focusing excites subwavelength phononic eigenmodes in the resonator lattice, enabling the subwavelength focusing. This method resulted in a focus resolution of $\lambda/8$, which was improved to $\lambda/25$ using iterative TR methods. With a similar experimental setup, Maznev *et al*.[41] established that as the frequency of the time aligned waves approaches that of the resonance frequency of an individual Helmholtz resonator (420 Hz), the spatial resolution increases. They showed that the resonator array acts as an effective medium that decreases the effective wavelength of waves below the Helmholtz resonance. Their work also demonstrated that TR was not necessary for subwavelength focusing in this configuration. Kingsley *et al*.[37] explored the tradeoff in resolution of TR focusing among an array of resonators versus the amplitude of that focusing, the impact of the resonator shape on these factors, and the dual-nature aspects of the array of resonators acting together as an effective medium and the discrete impacts of each resonator on the focusing using equivalent circuit modeling. Kingsley and Anderson[42] then verified this circuit model with finite-element, full-wave modeling and the ability of a single resonator to slow down passing waves was illustrated. Finally, Kingsley *et al.*[43] experimentally demonstrated that super resolution focusing with a resonator array is possible in a reverberant environment and showed that it could be used to image multipole sources.

Aside from the work reviewed above by Kingsley *et al.*, all previous work with the soda can arrangement was restricted to direct sound arrivals from in-plane sources. Lerosey *et al.* utilized a reverberant electromagnetic environment, but resonator array experiments haven't been done much in acoustic reverberant environments, other than Kingsley's work. Kingsley *et al.*[43] used sources that were not in plane and utilized significant reverberation in their TR experiments (the same as we will do here). The degree to which super resolution depends on the angle of incidence of the focused waves has not yet been explored. Obviously the focusing is achievable

with in-plane waves as demonstrated by Lemoult *et al.* and Maznev *et al.* and the inclusion of out-of-plane waves doesn't prevent super resolution focusing as demonstrated by Lerosey *et al.* and Kingsley *et al.* but does the inclusion of out-of-plane waves improve or hamper the resolution, and if it hampers the resolution, are there ways to restrict the focused waves to those in plane?

The purpose of this work is to fill in some of these gaps by reexamining TR focusing among a soda can array in a reverberation chamber by imposing a physical waveguide and using wave field decomposition to restrict waves to those in plane. Subwavelength focusing is achievable, though to a lesser degree, using a soda can array in the reverberation chamber with a 3D aperture (of incident waves). It is then demonstrated experimentally that focus resolution improves further by encasing the soda can array in a 2D waveguide, blocking incident waves from out-of-plane with the resonator array. Next, using calculated particle velocity components of experimentally obtained data, a partial pressure field excluding the z-component of particle motion is shown to further improve the spatial resolution of the focus, showing that the components of the incident signal that are in-plane with the resonator array are preferred for maximizing the resolution of the focus. A vertical characterization of the spatial extent of the focusing outward from the soda can array is also provided.

Chapter 2

Experimental Setup

All experiments are performed in the large reverberation chamber at Brigham Young University having dimensions of 4.96 x 5.89 x 6.98 m. Its overall reverberation time is 6.85 s and its Schroeder frequency is 355 Hz, above which the chamber is assumed to contain a diffuse field. In these experiments, eight HR824mk2 Mackie (Seattle, WA) loudspeakers are placed randomly around the perimeter of the chamber. An example of their arrangement is shown in Fig. 2.1(a). The loudspeakers are intentionally pointed away from the focal location to maximize the impact of the reverberation in the reversed impulse responses.[44] Figure 2.1(a) also shows a mechanical scanning gantry with two dimensions each controlled by an Applied Motion Products STAC 6i (Morgan Hill, CA) controller and an Applied Motion Products HT23-550D stepper motor. The translation stage of the gantry has dimensions of 2 x 2 m and holds a GRAS 46AQ (Holte, Denmark) 1.27 cm (1/2 in.) random-incidence microphone used to iteratively probe the spatial extent of a wave field of interest in two dimensions. The microphone is powered by a GRAS 12AX CCP power module.

The TR experiments are performed using a computer with three Spectrum Instrumentation (Grosshansdorf, Germany) PCI cards, two M2i.6022 generator cards (containing one channel for each of the eight loudspeakers) and one M2i.4931 acquisition card for the microphone receiver. All channels on the generator and acquisition cards are time synchronized using a Spectrum Star-Hub module. ESTR,[45] a LabVIEW-based software, is used as a user interface to operate the cards,

the acoustic equipment, the mechanical scanning gantry, and efficiently perform TR experiments.

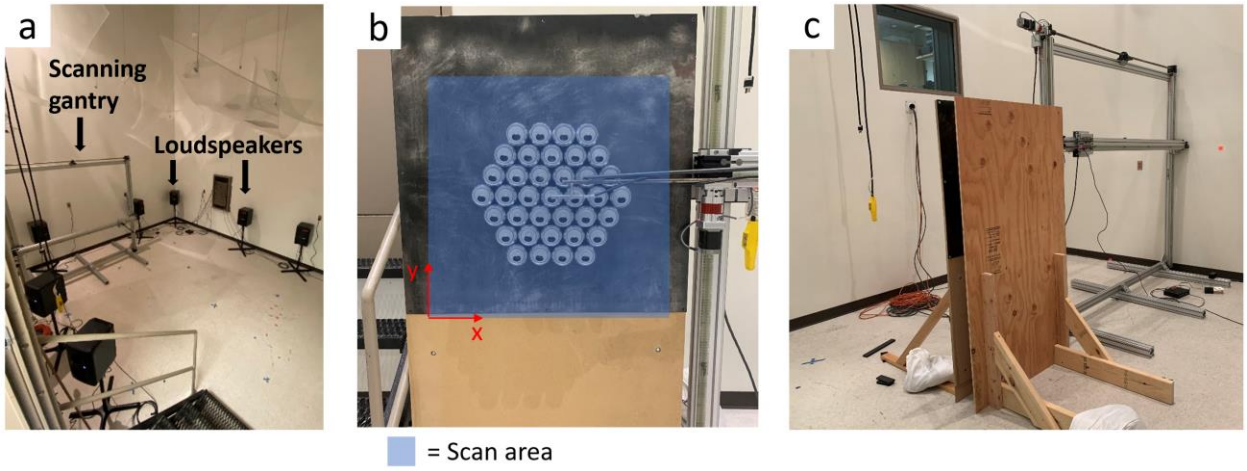

FIG. 2.1. (a) Photograph of the reverberation chamber with 7 of the loudspeakers visible, along with the microphone scanning gantry. (b) Photograph of the microphone arm from the scanning apparatus (visible on the right) with the soda can array, with the microphone placed at the focus position above the center can. The blue area depicts the area over which the scan of the focus is performed. The Cartesian reference frame used to discuss the apparatus and results is defined with the red arrows and text. (c) Photograph of the physical two-dimensional waveguide used to restrict out-of-plane incidence angles.

An example of the implementation of a TR experiment is Illustrated in Fig. 2.2. With the receiver placed in the user-selected focus position, a two-second duration, linear chirp signal (360-420 Hz) with some buffering zeros (Fig. 2.2(a)) is played from each loudspeaker individually and the response to each chirp are recorded (Fig. 2.2(b)). Figure 2.2(c) shows an example of a cross-correlated and time-reversed impulse response. All eight reversed impulse responses are broadcast simultaneously from the respective loudspeakers to create a TR focus, measured by the microphone receiver at the focus position. An example of a focus signal is shown in Fig. 2.2(d). A spatial characterization of the focus is simply obtained by repeating the measured focus while

measuring the field at different locations with the microphone, whose recordings are time synchronized.

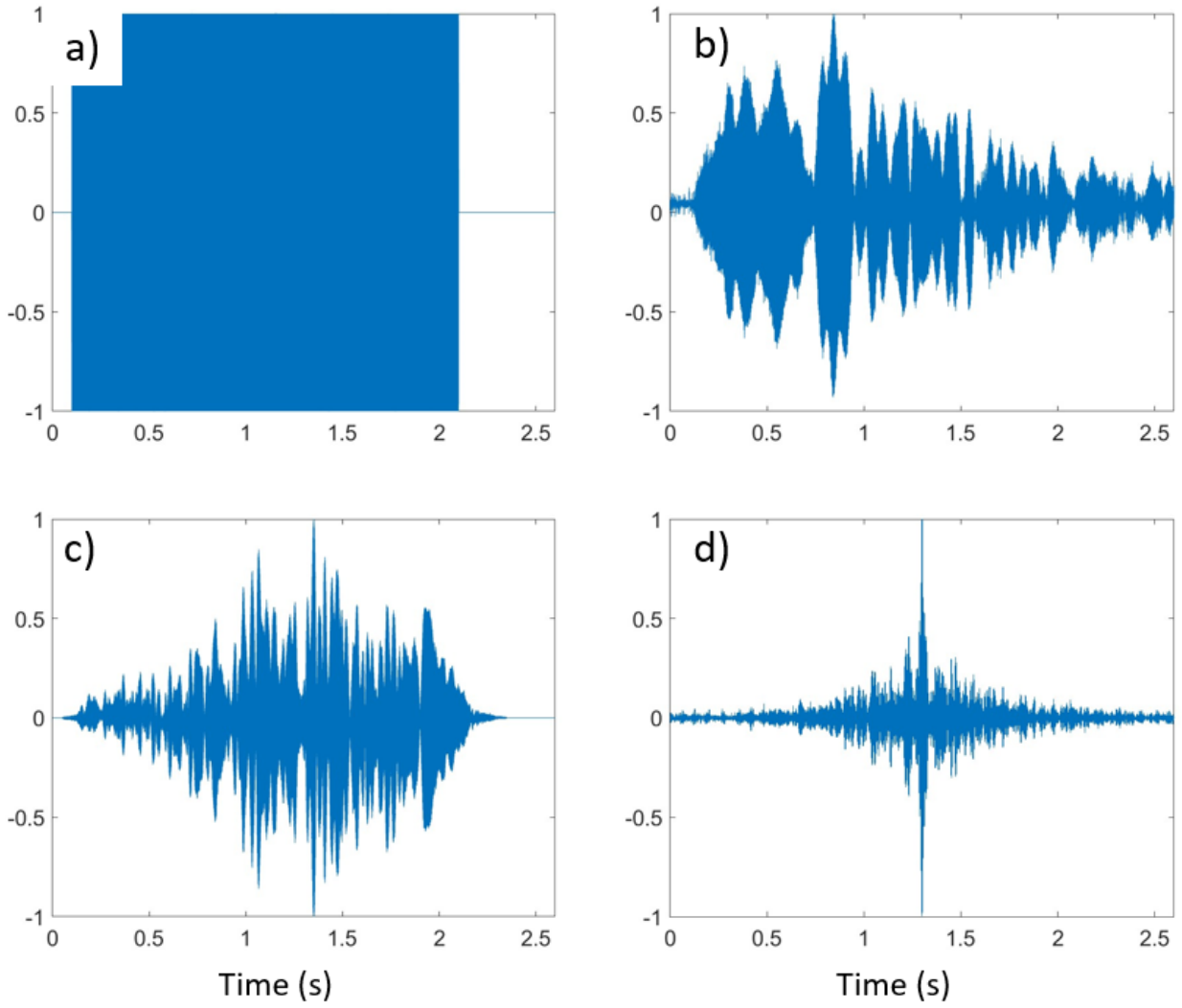

FIG. 2.2. Example signals for a time reversal (TR) experiment with normalized amplitudes. (a) The 360-420 Hz chirp signal played separately by each loudspeaker. (b) Example of a chirp response, recorded at the microphone placed at the focus location, unique for each loudspeaker. (c) A time-reversed cross correlation of the signal in part b. (d) A focus recorded at the focus location, generated as all loudspeakers play their corresponding signals from part c.

Just as previous experiments have used soda cans as Helmholtz resonators (420 Hz), this experiment follows suit, with 37 cans tightly arranged in a hexagonal array (pictured in Fig. 2.1(b)). The cans are magnetically mounted on a board with its plane perpendicular to the ground to accommodate the vertical orientation of the scanning gantry. The resonator array is elevated more than a meter above the floor to minimize unwanted amplitude increases from approaching a reflecting surface[46] and remain within the diffuse zone of the chamber.[47] Each spatial scan measured here consists of a 60 x 60 cm scan area with a grid spacing of 1 cm, which is large enough to measure the field above the entire resonator array; the 1 cm spacing was chosen since it is smaller than the opening of a can, thus ensuring we would always have a scan position above each can opening. In each scan, the focus is directed over the mouth of the center can in the array and the head of the microphone is 1 cm above the openings of the soda cans.

Although a maximal bandwidth is ideal, the bandwidth of 360-420 Hz used in this experiment was chosen because of the Schroeder frequency of the reverberation chamber and to stay below the resonance frequency of the individual resonators in the soda can array, which provide the lower and upper limit of bandwidth respectively. Below the Schroeder frequency (355 Hz), distortion from room mode excitation may occur, and above the resonant frequency of the soda cans (420 Hz), the waves are significantly attenuated and no longer experience the shorter effective wavelength that the resonator array is intended to produce.[42]

Chapter 3

Results

A. Focusing With and Without a Resonator Array

As a baseline measurement, the first experiment is a characterization of the spatial extent of the focusing when no array of cans is present at the focus position. The best possible resolution in this case would be that of the diffraction limit. A cross section of the instantaneous, squared sound pressure amplitude versus space is displayed in Fig. 3.1(a) at the time of maximal focusing (focal time). A squared sine wave of the highest frequency in the bandwidth, 420 Hz, is also plotted to illustrate the tightest possible resolution with this bandwidth. In this case the width of the no-can TR focusing is wider than that of the highest frequency, which is understandable since the focusing contains a finite bandwidth of frequencies, all of which have larger wavelengths than the highest frequency in the band. Additionally, the point spread function of the focused waves' aperture can often cause the TR focusing to be wider than the diffraction limit. The FWHM of the intensity of the highest frequency is 20.4 cm $= \lambda/4$. In this case the FWHM of the focusing is 38.1 cm, so $38.1/20.4 = 187\%$ of the diffraction limit.

Next a characterization of the spatial extent of a TR focus over the soda can array is given. Figure 3.1(b) displays x and y cross sections of the instantaneous squared pressure of the focus at focal time in comparison with the diffraction limit. The narrower FWHM of the two cross sections is 10.0 cm, which is $10.0/20.4 = 49.0\%$ (approximately $\lambda/4$) of the diffraction limit. This is not as well resolved as similar experiments that have been done in anechoic environments that reported

$\lambda/8 = 25\%$ of the diffraction limit.[40] However, in those experiments, the median frequency of the bandwidth (400 Hz) was used to define the diffraction limit, instead of using their highest frequency, 600 Hz. If the highest frequency were used, then it would be 38% (almost $\lambda/6$) of the diffraction limit. Thus, our results are 129% of their reported resolution and this can be attributed to the difference between an anechoic measurement (utilizing only the direct sound that arrives in plane) versus a reverberant measurement (utilizing a lot of reverberation in the impulse response, such that waves arrive from all angles of incidence).

B. Using a Physical 2D Waveguide

Kingsley *et al*. showed that phase lagging can occur for waves passing over resonators below the resonance frequency of a single resonator in a one-dimensional waveguide and hypothesized that these phase lags can effectively lead to a decrease in the effective phase speed of the resonator array allowing the sub-diffraction limited focusing.[42] Noting that such a setup can be extended to the two-dimensional waveguide, a parallel reflecting barrier wall with identical dimensions to the board holding the cans is placed about 6 cm above the openings of the soda cans to create a waveguide (see Fig. 2.1(c)), allowing space for the scanning microphone to fit between the soda cans and the barrier. The resulting distance between the boards is $L = 18$ cm. The additional board prevents waves from arriving perpendicular to the plane of the array and this waveguide also blocks unwanted cross mode propagation in the waveguide. The well-known waveguide cutoff frequency f_{01} defines the highest frequency at which plane waves can propagate within the waveguide (or the lowest frequency limit at which the first order cross mode propagates in the waveguide)[48] and is given by

$$f_{01} = \frac{c}{2L}, \tag{1}$$

where $c = 343$ m/s defines wave speed and waveguide spacing L is smaller than the other dimensions of the waveguide. For this waveguide, $f_{01} = 953\ Hz$, much greater than $420\ Hz$, the highest frequency in the bandwidth. The soda cans are placed in the center of the waveguide to avoid the evanescent propagation of cross modes into the waveguide, which typically only propagate into the waveguide a distance corresponding to the 18 cm waveguide dimension. Acoustic waves passing over the soda cans within the waveguide are thus assumed to be plane waves and propagate only in plane.

When the waveguide is added to the setup, the spatial extent of the TR focusing over the resonator array notably reduces down to 5.7 cm, a 43% improvement compared to the focusing among the resonator array without the waveguide present. This corresponds to 28% (almost $\lambda/8$) of the diffraction limit.

C. Numerical 2D Waveguide

Due to the practical limiting nature of using a two-dimensional waveguide in three-dimensional applications, we explore a method to replace its function while still improving the spatial focus resolution. The goal of this method is to mathematically impose a condition to remove the out-of-plane (z-directional) component in the wave field to approximate the acoustic behavior of the two-dimensional waveguide. When the spatial extent of the TR focus is measured in a two-dimensional array coplanar with the resonator array (in the x and y dimensions), a two-dimensional pressure gradient may be easily computed, but there is little direct information about the z-direction component (out-of-plane). However, a processing technique using a combination of well-known linearized equations in acoustics allows us to disregard the z component of particle motion.

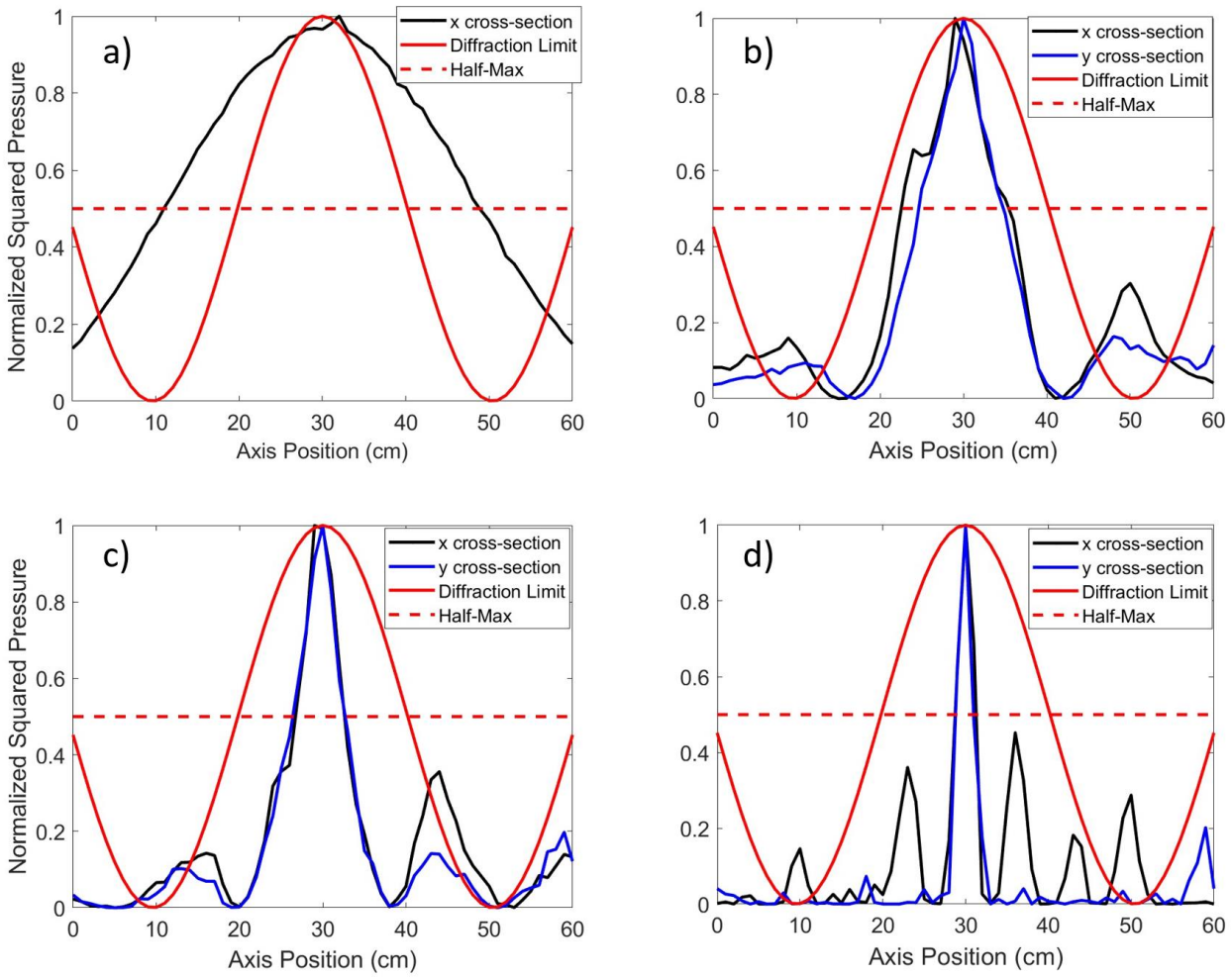

FIG 3.1. A comparison of four different cases of time reversal focusing, showing cross sections of the spatial extent of the instantaneous squared pressure at focal time with amplitude normalized for comparison. (a) A TR focus in the reverb chamber with no cans present. (b) A TR focus over the soda can array. (c) A TR focus with the 2D waveguide and the soda can array. (d) A post-processing partial pressure reconstruction of a focus with the soda can array and no waveguide.

As shown by Ref. 49, Euler's equation,

$$\vec{u} = -\frac{1}{\rho_0}\int_0^t \vec{\nabla} p \, dt, \tag{2}$$

can be used to determine the components of particle velocity ($\vec{u}$) coplanar with the measured array, where ρ_0 is equilibrium fluid density, $\vec{\nabla}p$ is the gradient of the pressure, and dt is the time step of the pressure measurements. At this point, it does not matter that the z-component of particle velocity is unknown, because the desired $u_z = 0$ condition can be artificially imposed, which simulates the physical effect of a two-dimensional waveguide. Although the motion of the air in the resonators will be mostly z-directional, it is the information carried in-plane with the resonator array, modified by the superoscillatory effects (subwavelength phononic eigenmodes) of the resonator array, that contributes to the super resolution [2,6].

Next, the equation of continuity,

$$\frac{d\vec{\rho}}{dt} = -\rho_0 \, \vec{\nabla} \cdot \vec{u} \, , \tag{3}$$

and the equation of state,

$$p = \rho \, c^2, \tag{4}$$

can be combined into an Eq. (5), which will allow us to use the previously obtained velocity components in a reconstruction of a partial pressure field (having only x and y components)[50] with the newly imposed condition of invariance in the z direction. This reconstructed, partial pressure field constitutes what our measurement array would theoretically have measured had there been a two-dimensional waveguide physically present,

$$\frac{1}{c^2}\frac{d\vec{\rho}}{dt} = -\rho_0 \left[\frac{du_x}{dx} + \frac{du_y}{dy} + \frac{du_z}{dz}\right],$$

$$p = -\rho_0 \, c^2 \int_0^t \left[\frac{du_x}{dx} + \frac{du_y}{dy} + \frac{du_z}{dz}\right] dt \, , \tag{5}$$

where it is assumed that $\frac{du_z}{dz} = 0$.

Applied to experimental data, as shown in Fig. 3.1(d), this method yields a reconstructed focus with a FWHM of 2.1 cm, which constitutes a 79% improvement in spatial resolution over

the original data measured over the soda can array, and a 63% improvement over using a physical waveguide, allowing the TR focus to clearly distinguish an individual resonator in the array. It also represents a focusing that is 10% of the diffraction limit (approximately $\lambda/20$).

D. z Extent of Focusing

Finally, a characterization of the vertical extent of a focus over the soda can array (with no waveguide or post-processing performed) is given, which to the authors' knowledge has not been presented by others. A two-dimensional spatial scan in the (y, z) plane is aligned with a row of cans in the array, the TR focus is directed at the mouth of the center can (at $y = 30$ and $z = 0$), and the pressure wave field is measured (a plane perpendicular to the resonator array). Figure 3.2(a) shows a plot of the instantaneous squared pressure map at the focus time and a visible evanescent decay of the focus moving outward from the resonator array is apparent in the z direction, with individual resonators indistinguishable more than about 3 cm from the openings of the soda cans. Figure 3.2(b) is a profile of the squared pressure along the z-axis directly out from the focus. Comparing the z extent of the focus against the diffraction limit shows a focal width that is 2.0 cm, 9.8% (better than $\lambda/20$) of the diffraction limit.

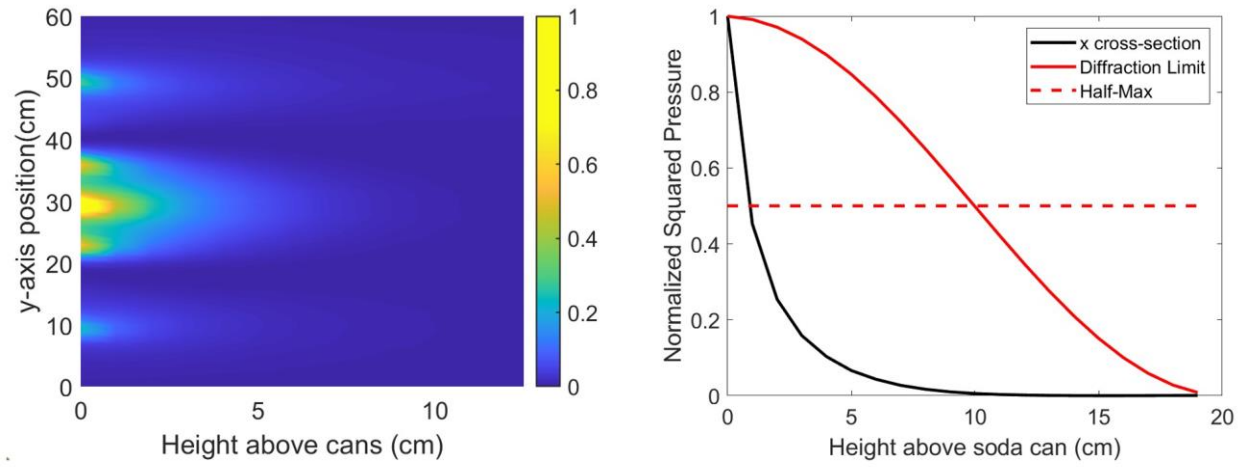

FIG. 3.2. (a) A vertical plane view in the (y, z) plane of the spatial distribution of the instantaneous squared pressure map at the focus time of a TR focus over the soda can array. (b) A cross-section view of the z-extent of the focus compared against the diffraction limit.

Chapter 4

Conclusion

The contributions of the z component of the focal wave field has been explored. Previous results that used only the direct sound were 129% better in comparison to results in a reverberant environment. A similar experiment performed by Lemoult *et al*.[40] was able to achieve a resolution 38% of the diffraction limit (using our definition or 25% using their definition), while the resolution achieved in the case of this experiment just over the soda cans was approximately 49% of the diffraction limit. The discrepancy here is explained by the wider aperture of the focusing with incident angles arriving in out-of-plane directions in the focusing from the reverberant environment.

Using a two-dimensional waveguide parallel with the soda can array plane, the dependence of aperture (incidence angle) is demonstrated, showing that the focus waves propagating in the resonator array plane are better suited to provide higher-resolution focusing than those coming from other incident angles (particularly the out of plane direction). The physical waveguide produces a resolution 28% of the diffraction limit (nearly $\lambda/8$). Using a physical two-dimensional waveguide is not always practical for many focusing applications, however. To further build upon this principle, it is shown that the physical 2D waveguide is not necessary when it is possible to measure the spatial extent of the focusing in a two-dimensional plane above the soda can array. A process using the decomposition of particle velocities and reconstructing a partial pressure field, while excluding the out-of-plane component of particle movement, can artificially imitate the

effect of a 2D waveguide, and using this process on the focus measured over the soda cans significantly improves the resolution of the signal (a 79% improvement), resulting in a resolution 10% of the diffraction limit (approximately $\lambda/20$).

Finally, it is shown that the spatial extent of the focus in the out-of-plane direction relative to the soda can array plane has exceptional resolution (without a waveguide or post-processing of the data), which is 9.8% (better than $\lambda/20$) of the diffraction limit. This is due to the exponential decay of amplitude with distance as you move away from the mouth of the soda can.

As Maznev *et al.*[35] asserted, we also suggest that the physics of the diffraction limit are not technically violated in these experiments. Relative to TR focusing in free space (away from the resonator array) we have achieved much better focusing, but the boundary conditions have been greatly changed due to the soda can array, so the effective wavelength is much smaller due to these boundary conditions. However, the soda can array can be thought of as an effective medium modifying the phase and/or wavelength of the incident waves of the focus, making it possible to achieve a superior focus resolution than what would otherwise be possible in free space. This can be useful across many focusing and imaging/source reconstruction applications.

References

[1] P. N. Keating, T. Sawatari and G. Zilinskas, “Signal processing in acoustic imaging,” *Proceedings of the IEEE* **67**(4), 496-510 (1979).

[2] M. Kompis, H. Pasterkamp, and G. R. Wodicka, “Acoustic imaging of the human chest,” *Chest* **120**(4), 1309-1321 (2001).

[3] M. Born, E. Wolf, A. B. Bhatia, P. C. Clemmow, D. Gabor, A. R. Stokes, P. A. Wayman, W. L. Wilcock, and P. L. Knight, *Principles of Optics*, (Cambridge University Press, Cambridge, U.K., 2020).

[4] M. Fink, “Time reversed acoustics,” *Phys. Today*, **50**(3), 34-40 (1997).

[5] B. E. Anderson, M. Griffa, C. Larmat, T. J. Ulrich, and P. A. Johnson, “Time reversal*,” Acoust. Today* **4**(1), 5-16 (2008).

[6] B. E. Anderson, M. C. Remillieux, P.-Y. Le Bas, and T. J. Ulrich, *“Time reversal techniques,” Chapter 14 in Nonlinear Acoustic Techniques for Nondestructive Evaluation*, 1st Edition, Editor Tribikram Kundu, ISBN: 978-3-319-94476-0 (Springer and Acoustical Society of America, New York, 2018), pp. 547-581.

[7] B. Van Damme, K. Van Den Abeele, Y. Li, and O. Bou Matar, “Time reversed acoustics techniques for elastic imaging in reverberant and nonreverberant media: An experimental study of the chaotic cavity transducer concept,” *J. Appl. Phys*. **109**(10), 104910 (2011).

[8] B. E. Anderson, M. Clemens, and M. L. Willardson, “The effect of transducer directivity on time reversal focusing,” *J. Acoust. Soc. Am.* **142**(1), EL95–EL101 (2017).

[9] A. Parvulescu, and C. S. Clay, "Reproducibility of signal transmissions in the ocean," *Radio and Electronic Engineer,* **29**(4), 223-228 (1965).

[10] D. R. Jackson and D. R. Dowling, "Phase conjugation in underwater acoustics," *J. Acoust. Soc. Am.* **89**, 171–181 (1991).

[11] G. F. Edelmann, H. C. Song, S. Kim, W. S. Hodgkiss, W. A. Kuperman, and T. Akal, "Underwater acoustic communications using time reversal," *IEEE J. Ocean Eng.* **30**(4), 852–864 (2005).

[12] H. C. Song, "An overview of underwater time-reversal communication," *IEEE J. Ocean. Eng.* **41**, 644–655 (2016).

[13] H. C. Song and W. A. Kuperman, "Time machine in ocean acoustics," *J. Acoust. Soc. Am.* **153**(1), R1-R2 (2023).

[14] J. V. Candy, A. W. Meyer, A. J. Poggio, and B. L. Guidry, "Time-reversal processing for an acoustic communications experiment in a highly reverberant environment," *J. Acoust. Soc. Am.* **115**(4), 1621–1631 (2004).

[15] S. Yon, M. Tanter, and M. Fink, "Sound focusing in rooms: The time-reversal approach," *J. Acoust. Soc. Am.* **113**(3), 1533–1543 (2003).

[16] G. Ribay, J. de Rosny, and M. Fink, "Time reversal of noise sources in a reverberation room," *J. Acoust. Soc. Am.* **117**(5), 2866–2872 (2005).

[17] B. E. Anderson, T. J. Ulrich, P.-Y. Le Bas, and J. A. Ten Cate, "Three dimensional time reversal communications in elastic media," *J. Acoust. Soc. Am.* **139**(2), EL25-EL30 (2016).

[18] B. E. Anderson, "High amplitude time reversal focusing of sound and vibration," *Proc. Meet. Acoust.,* accepted and in press.

[19] J.-L. Thomas, F. Wu, and M. Fink, "Time reversal focusing applied to lithotripsy," *Ultrason. Imag.* **18**(2), 106–121 (1996).

[20] M. Tanter, J.-L. Thomas, and M. Fink, "Focusing and steering through absorbing and aberrating layers: Application to ultrasonic propagation through the skull," *J. Acoust. Soc. Am.* **103**(5), 2403–2410 (1998).

[21] G. Montaldo, P. Roux, A. Derode, C. Negreira, and M. Fink, "Ultrasound shock wave generator with one-bit time reversal in a dispersive medium, application to lithotripsy," *Appl. Phys. Lett.* **80**, 897–899 (2002).

[22] B. E. Anderson, M. Griffa, T. J. Ulrich, P.-Y. Le Bas, R. A. Guyer, and P. A. Johnson, "Crack localization and characterization in solid media using time reversal techniques," *Am. Rock Mech. Assoc.*, #10-154 (2010).

[23] M. L. Willardson, B. E. Anderson, S. M. Young, M. H. Denison, and B. D. Patchett, "Time reversal focusing of high amplitude sound in a reverberation chamber," *J. Acoust. Soc. Am.* **143**(2), 696-705 (2018).

[24] C. B. Wallace and B. E. Anderson, "High-amplitude time reversal focusing of airborne ultrasound to generate a focused nonlinear difference frequency," *J. Acoust. Soc. Am.* **150**(2), 1411-1423 (2021).

[25] B. D. Patchett and B. E. Anderson, "Nonlinear characteristics of high amplitude focusing using time reversal in a reverberation chamber," *J. Acoust. Soc. Am.* **151**(6), 3603-3614 (2022).

[26] B. D. Patchett, B. E. Anderson, and A. D. Kingsley, "Numerical modeling of Mach-stem formation in high-amplitude time-reversal focusing," *J. Acoust. Soc. Am.* **153**(5), 2724-2732 (2023).

[27] C. Larmat, J.-P. Montagner, M. Fink, Y. Capdeville, A. Tourin, and E. Clevede, "Time-reversal imaging of seismic sources and applications to the great Sumatra earthquake," *Geophys. Res. Lett.* **33**(19), L19312 (2006).

[28] C. Larmat, J. Tromp, Q. Liu, and J.-P. Montagner, "Time-reversal location of glacial earthquakes," *J. Geophys. Res.* **113**(B9), B09314 (2008).

[29] C. Larmat, R. A. Guyer, and P. A. Johnson, "Tremor source location using time-reversal: selecting the appropriate imaging field," *Geophys. Res. Lett.* **36**(22), L22304 (2009).

[30] C. S. Larmat, R. A. Guyer, and P. A. Johnson, "Time-reversal methods in geophysics," *Phys. Today* **63**(8), 31–35 (2010).

[31] R. K. Ing and N. Quieffin, "In solid localization of finger impacts using acoustic time-reversal process," *Appl. Phys. Lett.* **87**(20), 204104 (2005).

[32] D. Vigoureux and J.-L. Guyader, "A simplified time reversal method used to localize vibrations sources in a complex structure," *Appl. Acoust.* **73**(5), 491–496 (2012).

[33] D. G. Albert, L. Liu, and M. L. Moran, "Time reversal processing for source location in an urban environment (L)," *J. Acoust. Soc. Am.* **118**(2), 616–619 (2005).

[34] S. Cheinet, L. Ehrhardt, and T. Broglin, "Impulse source localization in an urban environment: time reversal versus time matching," *J. Acoust. Soc. Am.* **139**(1), 128–140 (2016).

[35] A. A. Maznev and O. B. Wright, "Upholding the diffraction limit in the focusing of light and sound," *Wave Mot.* **68**, 182–189 (2017).

[36] E. D. Golightly, B. E. Anderson, A. D. Kingsley, R. Russell, and R. Higgins, "Super resolution, time reversal focusing using path diverting properties of scatterers," *Appl. Acoust.* **206**, 109308 (2023).

[37] A. D. Kingsley, B. E. Anderson, and T. J. Ulrich, "Super-resolution within a one-dimensional phononic crystal of resonators using time reversal in an equivalent circuit model," *J. Acoust. Soc. Am.* **152**(3), 1263-1271 (2022).

[38] G. Lerosey, J. de Rosny, A. Tourin, and M. Fink, "Focusing beyond the diffraction limit with far-field time reversal," *Science* **315**(5815), 1120–1122 (2007).

[39] F. Lemoult, M. Fink, and G. Lerosey, "Acoustic resonators for far-field control of sound on a subwavelength scale," *Phys. Rev. Lett.* **107**(6), 064301 (2011).

[40] F. Lemoult, N. Kaina, M. Fink, and G. Lerosey, "Soda cans metamaterial: A subwavelength-scaled phononic crystal," *Crystals,* **6**(7) 82 (2016).

[41] A. A. Maznev, G. Gu, S. Y. Sun, J. Xu, Y. Shen, N. Fang, and S. Y. Zhang. "Extraordinary focusing of sound above a soda can array without time reversal," *New J. Phys.*, **17**(4), 042001 (2015).

[42] A. D. Kingsley and B. E. Anderson, "Time reversal in a phononic crystal using finite-element modeling and an equivalent circuit model," *JASA Exp. Lett*. **2**(12), 124002 (2022).

[43] A. D. Kingsley, A. Basham, and B. E. Anderson, "Time reversal imaging of complex sources in a 3-dimensional environment using a spatial inverse filter," *J. Acoust. Soc. Am*., under review.

[44] B. E. Anderson, M. Clemens, and M. L. Willardson, "The effect of transducer directionality on time reversal focusing," *J. Acoust. Soc. Am.* **142**(1), EL95-El101 (2017).

[45] A. D. Kingsley, J. M. Clift, B. E. Anderson, J. E. Ellsworth, T. J. Ulrich, and P.-Y. Le Bas, "Development of software for performing acoustic time reversal with multiple inputs and outputs," *Proc. Meet. Acoust*. **46**, 055003 (2022).

[46] B. D. Patchett, B. E. Anderson, and A. D. Kingsley, "The impact of room location on time reversal focusing amplitudes," *J. Acoust. Soc. Am*. **150**(2), 1424-1433 (2021).

[47] ISO 3741:2010, “Sound power and energy in reverberant environments” (International Organization for Standardization, Geneva, Switzerland, 2010).

[48] S. M. Young, B. E. Anderson, R. C. Davis, R. R. Vanfleet, N. B. Morrill, “Sound transmission measurements through porous screen” *Proc. Meet. Acoust.* **26**, 045003 (2017).

[49] F. J. Fahy, *Sound Intensity*, 2nd ed. (E&FSpon, London, 1995), p. 95.

[50] J. S. Lawrence, K. L. Gee, T. B. Neilsen and S. D. Sommerfeldt, “Highly directional pressure sensing using the phase gradient,” *J. Acoust. Soc. Am.* **144**(4), EL346-EL352 (2018).